Gamma and conversion electron spectroscopy using GABRIELA

R. Chakma, K. Hauschild, A. Lopez-Martens, A.V. Yeremin, O.N. Malyshev, A.G. Popeko, Yu. A. Popov, A.I. Svirikhin, V.I. Chepigin, O. Dorvaux, et al.

Gamma and conversion electron spectroscopy using GABRIELA

R. Chakma[1], K. Hauschild[1], A. Lopez-Martens[1], A.V. Yeremin[2], O.N. Malyshev[2], A.G. Popeko[2], Yu.A. Popov[2], A.I. Svirikhin[2], V. I Chepigin[2], O. Dorvaux[3], B. Gall[3], and K. Kessaci[3]

[1]IJCLab,IN2P3-CNRS, Université Paris Saclay, 91400 Orsay, France
[2]Flerov Laboratory of Nuclear Reactions, JINR, 141 980 Dubna, Russia
[3]Université de Strasbourg, CNRS, IPHC UMR 7178, 67000 Strasbourg,France

11 June 2020

Abstract

GABRIELA (Gamma Alpha Beta Recoil Investigations with the Electromagnetic Analyzer) is a detection system installed at the focal plane of the SHELS (Separator for Heavy Elements Spectroscopy) recoil separator for gamma and internal conversion electron spectroscopy of heavy and superheavy nuclei. GABRIELA has recently been upgraded. The characteristics of the new setup are presented using the GEANT4 Monte Carlo simulation toolkit and validated against experimental results. The impact of summing on the gamma-ray and electron detection efficiencies is discussed.

1 Introduction

Superheavy nuclei are unique nuclear systems under large Coulomb forces owing their existence to strong quantum shell effects. The quest for the next proton and neutron spherical shell closures motivated the idea of 'the island of stability', where residing nuclides are predicted to have half-lives that vary over tens of orders of magnitude, possibly spanning the age of the earth [1]. Although there is a consensus across different theoretical models in the prediction of the next neutron shell closure at $N = 184$, the position of the next proton shell closure at either Z = 114, 120, or 126 remains controversial [2]. Despite evidence in the measured lifetimes of the heaviest nuclei synthesized (see the review [3]), the anticipated island of stability awaits discovery.

With the current state of technology, the lighter transfermium nuclei are relatively easier to synthesize as compared to their heavier counterparts. To reduce large extrapolations of the nuclear models to the island of stability, the study of the nature, sequence, and spacing of the states of the lighter heavy nuclei are pertinent. Hitherto the spectroscopic data in the transfermium region remain sparse (see fig. 1 of ref. [4]). Constant efforts are underway in major experimental facilities around the globe. Recent developments in nuclear spectroscopy techniques and instrumentation have allowed the identification of single-particle and collective states in many heavy systems. To study the structure in detail, two techniques are currently employed: the first one is prompt spectroscopy at the target [4], generally performed using the recoil decay tagging method (RDT) [5, 6]. The other complementary technique is decay spectroscopy either at the focal plane of a recoil separator or at a decay station coupled to a gas-jet transport system [7] where alpha, gamma, and internal conversion electron spectroscopy of superheavy nuclei and their daughter products is performed. Gamma spectroscopy has been carried out for a few transfermium nuclei. However, in heavy nuclei, the emission of internal conversion electrons is a competitive de-excitation mode. Thus, conversion electron spectroscopy is a necessary supplementary technique to gamma spectroscopy, in studying the structure of heavy nuclei. The GABRIELA [8] setup at the focal plane of SHELS [9] in Dubna, Russia is aimed at performing detailed alpha, gamma, and conversion electron spectroscopy in the transfermium region. Since the beginning of the project in 2003, the decay properties of several nuclei have been studied (see refs. [10, 11, 12, 13, 14]) or are being investigated. The detection setup is gradually being modernized and upgraded. This paper discusses the current configuration of GABRIELA in sect. 2; the experimental setup's instrumentation is discussed in sect. 3; in sect. 4 the performance of GABRIELA as estimated using the GEANT4 Monte Carlo simulation code is presented; a validation study using in-beam data is seen in sect. 6 and finally, the conclusions are presented in sect. 7.

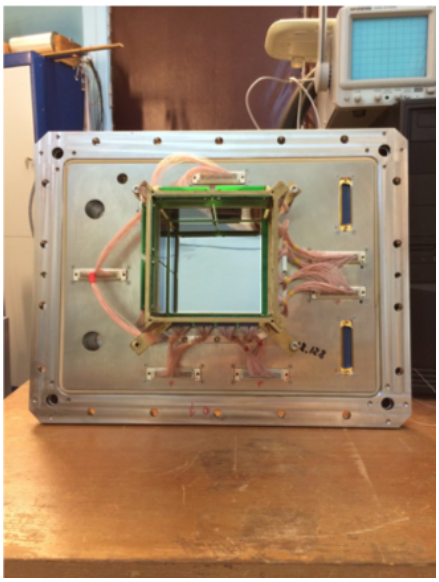

(a)

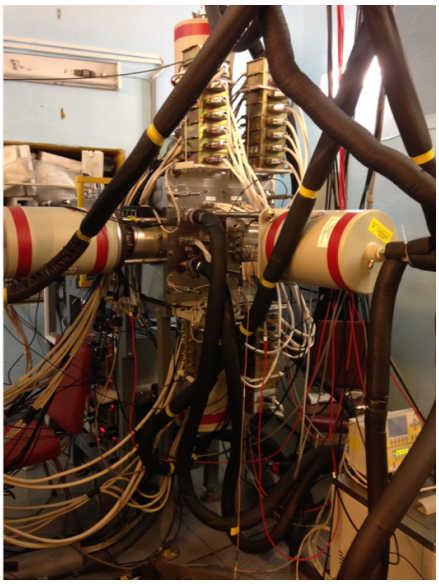

(b)

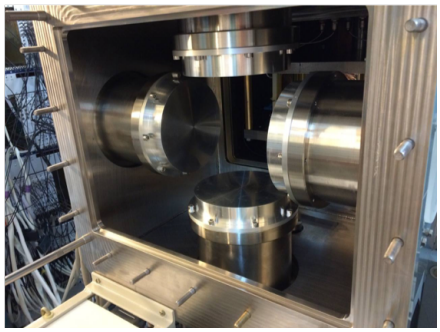

(c)

Figure 1: Photographs showing the components of the GABRIELA setup: a) Implantation detector and tunnel DSSDs b) Ge array and c) Inside of the vacuum chamber showing 4 of the 5 inserts.

2 Experimental Setup

At the Flerov Laboratory of Nuclear Reactions (FLNR), the U400 cyclotron delivers beams with intensities close to $p\mu A$ which impinge on a rotating target. Nuclei produced in fusion evaporation reactions are filtered and transported through the recoil separator SHELS [9] and delivered into the GABRIELA [8] detection system. In the following subsections, the current version of GABRIELA is described and parallels have been drawn wherever necessary between the current and the previous configuration.

2.1 Implantation detector

The nuclei of interest pass through the emissive foils of a Time of Flight (ToF) detector, a degrador foil, and then are implanted shallowly into a double-sided silicon detector (DSSD) called the implantation detector (see fig. 1a). The ToF detector provides a "flag" to distinguish the recoil implants from the subsequent decays in the implantation detector. The DSSD is a 100.4 $\times$ 100.4 mm^2 detector with 128 vertical and 128 horizontal strips, providing 16384 pixels for time and position correlations. DSSDs of varying thickness (300 μm and 500 μm) have been used. In its earlier version, the implantation detector of GABRIELA consisted of a smaller area 16-resistive-strip silicon detector [15].

2.2 Silicon detector array for *conversion electron*-spectroscopy

In the upstream direction of the implantation detector, an array of 8 small DSSDs is arranged in a tunnel configuration (see fig. 1a) supported by a cooling brass frame. They detect the alpha particles, electrons, and fission fragments, which escape from the implantation detector. Each of the 50×60 mm^2 tunnel detectors is ~ 0.7 mm thick and has 16 horizontal and 16 vertical strips. In the previous setup, four 4-strip silicon detectors were used instead, each having a thickness of 0.5 mm and a dimension of 50×50 mm^2 [15].

2.3 Germanium detector array for gamma-spectroscopy

Four coaxial, cylindrical, large volume Hyper Pure Germanium (HPGe) detectors are placed on each lateral side of the implantation detector and one clover [16] behind it (see fig. 1b). Two of the coaxial detectors are 73.1 mm long and have a diameter of 72.9 mm, while the 2 others are slightly smaller in size with a length and diameter of 71.9 mm and 72 mm respectively. The clover consists of four tapered crystals, each 50 mm in diameter and 70 mm long. Each Ge detector has an uncollimated $Bi_4Ge_3O_{12}$ (BGO) Compton shield. Special inserts into the vacuum chamber with 1 mm thick Aluminum windows (see fig. 1c) allow the Ge detectors to be placed close to the implantation detector. The BGO shields are used to improve the peak-to-total (P/T) ratio by rejecting the gamma-ray events which Compton

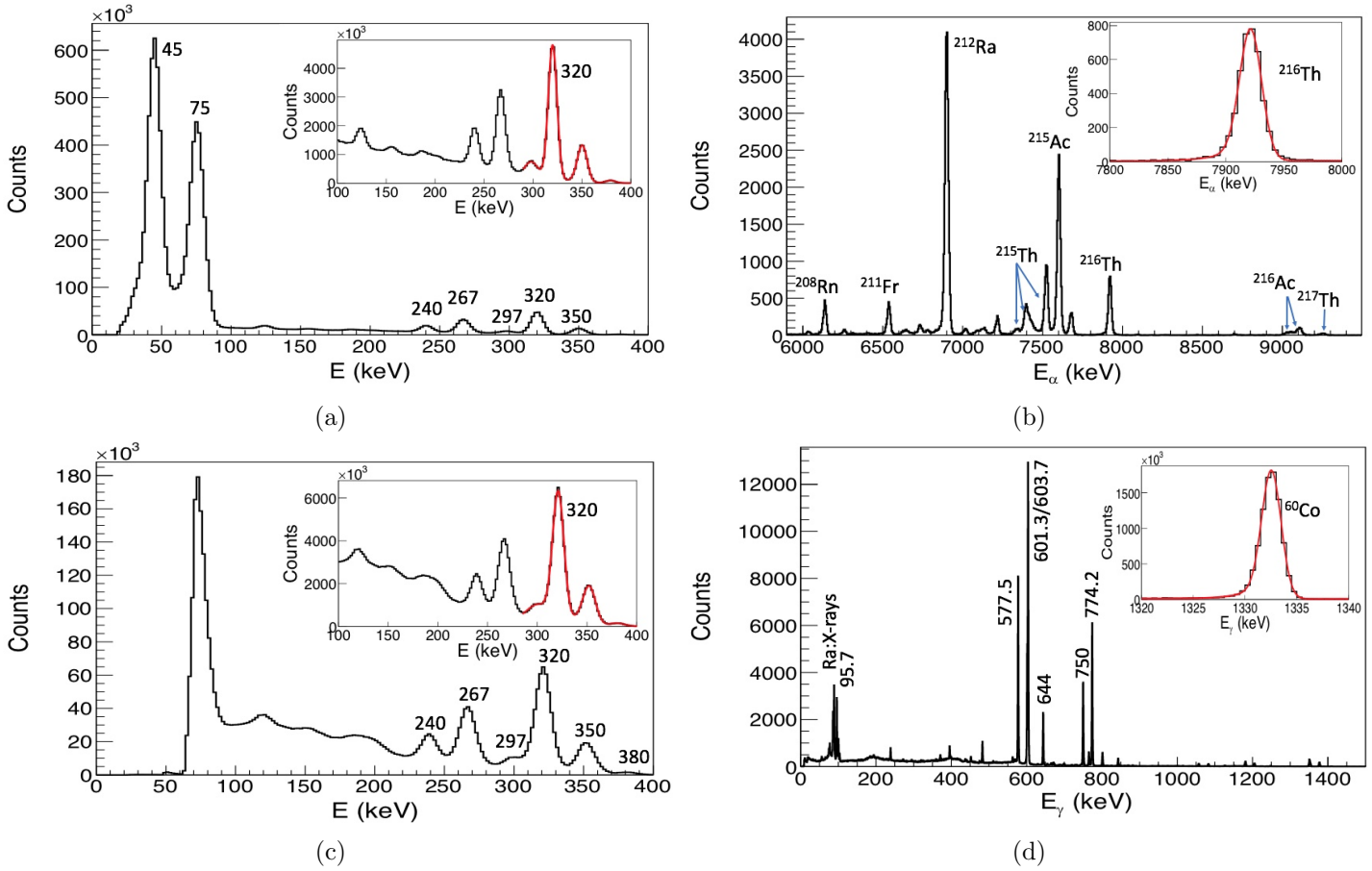

Figure 2: The energy spectra of the electrons emitted from a ^{133}Ba source detected in all the strips of a) the implantation detector and c) the tunnel detectors. b) Spectrum of alpha-particle energies emitted by the nuclei produced in the reaction ^{170}Er(^{50}Ti, xn yp). d) Energy spectrum of the Compton suppressed gamma rays detected within 24 μs from the implantation of ^{210}Ra nuclei. The insets in the figures show the corresponding fits (red curves) of the peaks, from which the resolutions of table 1 have been extracted. The histograms of the insets in figures a) and c) have been scaled by 100 to show their differences. The inset of figure d) shows the fit on the 1332.5 keV peak of ^{60}Co since gamma-ray resolutions are often quoted at this energy.

scatter out of the Ge detectors. This allows the identification of weak lines that could be overwhelmed by the Compton background of higher-energy and more intense lines. By filtering out radiation coming from the concrete walls, the background radiation rate is reduced, enabling increased "search" times for long-lived isomers. Experimentally, the average P/T is extracted from the gamma-ray spectrum due to a single transition (obtained by using either gamma or electron coincidences) by taking the ratio of the peak intensity over the intensity of the whole spectrum. The average P/T with beam on target was found to be 40-45%. In the previous setup, seven Eurogam Phase-I Ge detectors obtained from the French-UK loan pool surrounded the implantation detector and six of them were equipped with BGO shields.

3 Instrumentation

The signals from the silicon detectors are amplified with 2 different gains [17] for simultaneous measurement of conversion electrons from 70 keV to 2 MeV and alpha particles up to 25 MeV (another possibility is to measure alpha particles up to 25 MeV and fission fragments up to 140 MeV). For all the silicon detectors, 16-channel multiplexed analog-to-digital converters (ADCs) designed at FLNR are used. Every ADC datum is time-stamped with a 1 μs clock. Using a first-in, first-out buffer (FIFO), the average dead time of the ADCs has recently been reduced from $\sim$ 20-30 μs to $\sim$ 3-5 μs. The high gain data of the implantation detector and tunnel detectors are calibrated using a ^{133}Ba source (see figs. 2a, 2c). The low gain data of the implantation detector are calibrated using known alpha-emitting nuclei produced at the target and implanted into the implantation de-

tector (see fig. 2b). The Ge detectors are calibrated using standard calibration sources namely ^{60}Co, ^{133}Ba, ^{152}Eu, and checked with in-beam sources, for example, the isomeric decay of ^{210}Ra nuclei produced in the reaction ^{164}Dy(^{50}Ti, 4n)^{210}Ra (see fig. 2d). The resolutions and the typical thresholds of the detectors are given in table 1.

Detector	FWHM (keV)	Threshold (keV)
Implantation	10.8 ± 0.6 at 320 keV and 23.2 ± 1.7 at 7922 keV	40 - 60
Tunnel	14.4 ± 1.2 at 320 keV	60 - 100
Gamma	2.26 ± 0.17 at 1332.5 keV	∼15

Table 1: The resolutions and the typical thresholds of the GABRIELA detectors.

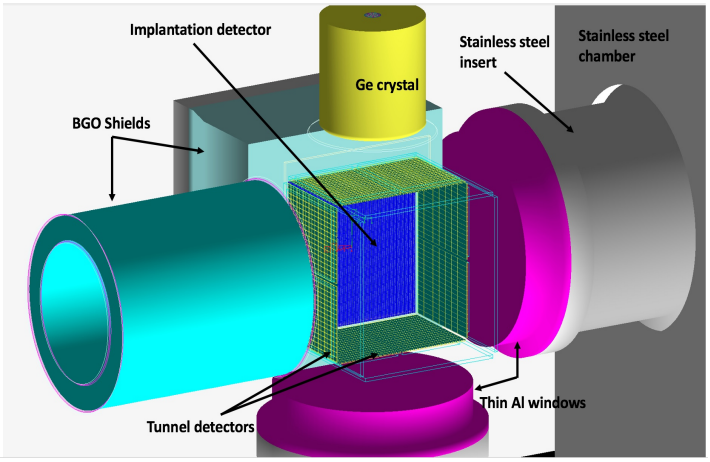

Figure 3: 3D rendering of the various elements of GABRIELA, as described in GEANT4.

4 GEANT4 Simulations

The software package for the simulation of radioactive decays in the GEANT4 [18] Monte Carlo simulation code is well established and was verified [19] against the Evaluated Nuclear Structure Data File (ENSDF) database [20]. User-defined photon evaporation files and radioactive decay files can be supplied to test different decay schemes. However, atomic relaxation processes are limited to $Z = 100$ in the current GEANT4 versions. To bypass this limitation different methods are used: one approach is to hard-code the whole atomic relaxation process as a part of the Primary Generator Action of GEANT4, while another method consists of disguising heavy nuclei as lighter ones (*i.e.* heaviest element available in GEANT4) by modifying their atomic properties [21, 22]. In this study, modifications in the GEANT4 source code were introduced to allow atomic relaxation processes up to *Rf* and the Auger and fluorescence data sets were extended up to $Z = 104$ by extrapolating the existing data in the range $90 \leq Z \leq 100$ using polynomial functions. The extrapolated values have been checked against the values given in the Table of Isotopes (TOI) [23].

The details of the geometry of the setup were built under the GEANT4 framework taking care of the active areas, the dead layers, and the gaps between the detectors. Other additional components such as the chamber, the PCB boards on which the silicon detectors are mounted, the support frame, etc. were also included in the GABRIELA's geometry construction (see the visualization in fig. 3). To emulate the electronics, multiplexing, missing channels, experimental resolutions, and typical thresholds were also added into the simulations.

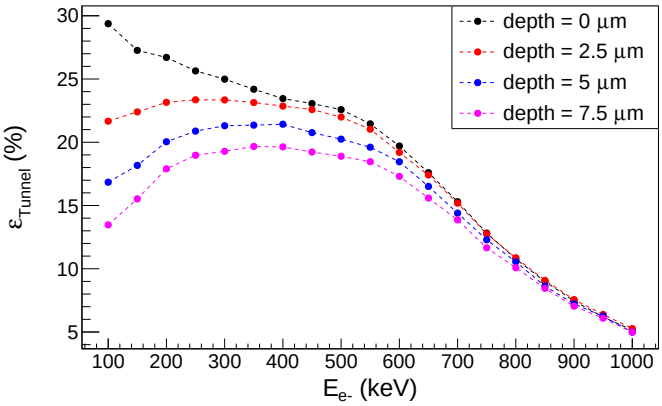

Figure 4: The simulated absolute efficiency of detecting electrons in the tunnel detectors emitted from a point source at various implantation depths in the implantation detector.

5 Efficiency Characterization

The response of a detector is dependent on the material, the position of the detector relative to the source, and on the nature and energy of the incoming particle.

To evaluate the efficiency of the Ge array and the tunnel detectors of GABRIELA, a number of simulations were performed by placing an isotropic gamma or electron source in the implantation detector. Two experimental XY (Z: beam direction) distributions (one, slightly off-centered, measured for ^{209}Ra during a calibration run and the other one centered, measured for ^{255}Rf during an experiment) and a point source centered

in the middle of the detector (X=Y=0) were used. Although almost no effect of the implantation depth (Z) on the gamma-ray detection efficiency was observed, a strong dependence of the electron efficiency was found, as can be seen in fig. 4. It is therefore important for every experiment to estimate the implantation depth profile of evaporation residues of interest.

5.1 Method to estimate the implantation depth of evaporation residues

Since the energy deposited by the alpha particles escaping the implantation detector is very sensitive to the thickness of the silicon they traverse, the Z distribution of the decaying nuclei can thereby be estimated from their energy spectrum. The implantation depth distribution is assumed to be Gaussian, motivated by the result of SRIM [24] calculations of the stopping of a parallel ^{238}U beam incident onto a silicon slab.

The experimental average implantation depth and the standard deviation, σ_{depth}, of the distribution was estimated by comparing the experimental spectrum of escaping alpha particles to simulated spectra obtained for different depths and standard deviations. The comparison was done by evaluating the following χ^2 test:

$$\chi^2 = \sum_{i=1}^{M} \left(\frac{N^i_{exp} - N^i_{sim}}{\sigma^i_{exp}} \right)^2 \quad (1)$$

where, M is the number of bins, N^i_{exp} and N^i_{sim} are the experimental and simulated number of counts in bin i respectively, and $\sigma^i_{exp} = \sqrt{N^i_{exp}}$.

As seen in fig. 5a, a clear minimum is obtained for an average implantation depth of 2.7 μm. Using this average depth and the standard deviation of 0.8 μm, which minimizes the χ^2 test, the energy spectrum of the escaping alpha particles emitted by ^{255}Rf (shown in fig. 5b) is well reproduced by the simulation. This implantation depth will be used in the following section to obtain the simulated gamma-ray and electron detection efficiencies of the HPGe array and tunnel detectors.

5.2 Electron and Gamma-ray efficiencies

The simulated efficiencies for a point source positioned at the center of the implantation detector and for the 2 distributed sources mentioned above are shown in figs. 6a and 6b). The energy depositions in each crystal of the clover detector [16] can be treated as separate events (singles mode) or can be summed in the so-called add-back mode. In this way, the full energy of the gamma rays, which scatter from one crystal to the neighboring one can be recovered. This procedure increases the clover efficiency by an add-back factor, which grows with gamma-ray energy. The asymptotic value of the add-back factor is found to be 1.52(1). In add-back mode, the absolute gamma-ray efficiency of GABRIELA peaks at 30% at 100 keV and drops to 8% at 1 MeV (63% of which comes from the contribution of the clover alone).

The efficiency of the tunnel detectors remains flat around 21% for electron energies ranging from 100 to 550 keV. The gradual loss of efficiency at higher electron energies is due to the finite thickness of the detector.

Compared to the previous version of GABRIELA, the simulated absolute gamma-ray detection efficiency of the present setup is found to be a factor of $\sim$ 3 - 4 higher, while the electron detection efficiency shows an increase of 5 - 7 %.

6 Validation

To check if the geometry constructed in GEANT4 is valid, a simple 2-transition cascade stemming from the 117 μs isomer of ^{209}Ra was used (see the level scheme of fig. 7a [27]). Experimentally, the isomeric gamma or internal conversion decays were selected by requiring that they occur between 16 to 956 μs after the implantation of ^{209}Ra nuclei. The upper limit was set to exclude the random correlations whereas the lower limit excludes the contribution from the decay of the 2.24 μs isomer in ^{210}Ra [29], which has very similar alpha-decay properties as ^{209}Ra. The experimental and simulated isomeric gamma-ray and conversion electron spectra are compared in figs. 8 and 9.

The gamma-ray and electron detection efficiencies can be measured using two methods. One is called the "singles method" as the values are measured from the singles spectra, while the other method is called the "coincidence method". In the coincidence method, the values are extracted from gamma-electron coincidences. The disadvantage of the singles method is that the number of decaying isomers (N_{isomer}) needs to be known, thus it cannot be applied to the experimental data. The efficiency values in the singles method are calculated using the following simple equations

$$\varepsilon(E) = \frac{N_{peak}}{N_{emitted}} \quad (2)$$

where, N_{peak} is the integral of the peak in the single spectrum and, $N_{emitted}$ for gamma rays and electrons are calculated as follows

$$N_{emitted,\gamma} = \frac{N_{isomer}}{(1+\alpha_{Tot})} \quad (3)$$

$$N_{emitted,Se-} = N_{isomer}\frac{\alpha_S}{(1+\alpha_{Tot})} \quad (4)$$

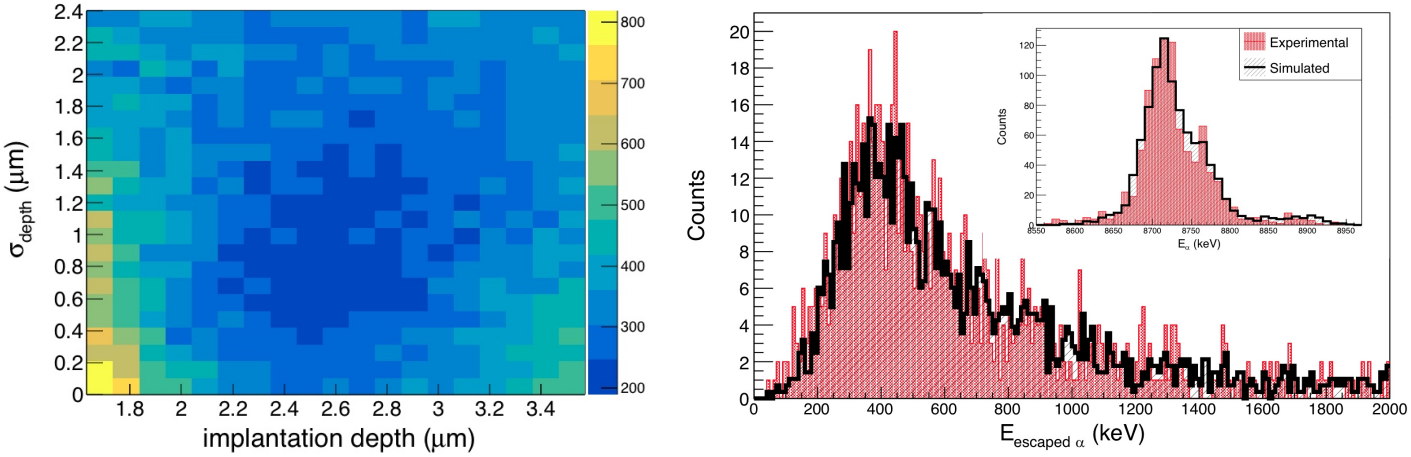

(a) (b)

Figure 5: a) Plot showing the χ^2 difference (see equation 1) between the experimental and simulated energy spectra of ^{255}Rf alpha particles that escape the DSSD as a function of the mean and the standard deviation of a Gaussian implantation depth distribution. b) Experimentally observed and simulated spectra of ^{255}Rf alpha particles at minimum χ^2 value. The inset shows the comparison of the alpha peaks in the spectra. In the simulation, the decay scheme of ^{255}Rf was taken from ref. [25] with alpha decay to additional levels [26].

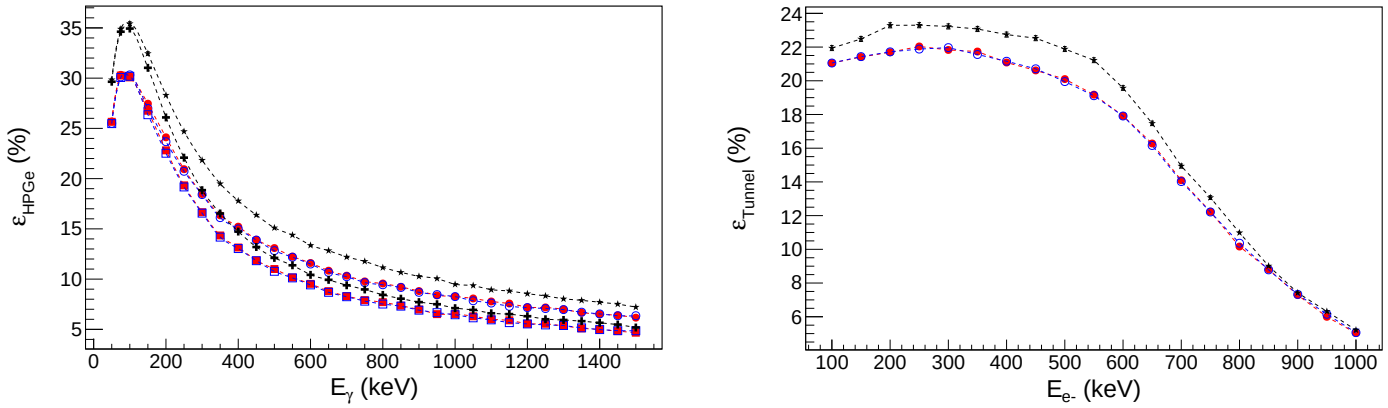

(a) (b)

Figure 6: The simulated absolute efficiency curves as a function of energy for different XY-distributions in the implantation detector with the same implantation depth profile, which minimizes the χ^2 test on the ^{255}Rf escaped alpha-particle energy spectra. a) Ge-array Compton-suppressed efficiencies for a point source in add-back mode ★ and in singles mode ✚, for the ^{209}Ra distribution in add-back mode ● and in singles mode ■, and for the ^{255}Rf distribution in add-back mode ○ and in singles mode □;b) Tunnel detector efficiencies in the case of a point source ★, for the ^{209}Ra ● and ^{255}Rf ○ distributions. Note that these simulated efficiency curves for ^{209}Ra and ^{255}Rf distributions lie practically on top of one another, indicating that similar position distributions of the radiation source do not affect the efficiencies.

where α is the internal conversion coefficient and S represents the shell from which the electron is emitted.

In the coincidence method, for two transitions $T1$ and $T2$ in coincidence the efficiency values are calculated using equations 5 and 6, where for instance, $\varepsilon_\gamma(T1_\gamma)$ is the absolute gamma-ray detection efficiency for gamma rays emitted in the T1 transition and $N(T1_\gamma \otimes T2_{Se^-})$ indicates the number of gamma rays emitted in the T1 transition detected in coincidence with electrons emitted from the shell S in the T2 transition.

$$\varepsilon_\gamma(T1_\gamma) = \frac{N(T1_\gamma \otimes T2_{Se^-})}{N(T2_{Se^-})}(1 + \alpha_{Tot}(T1)) \quad (5)$$

$$\varepsilon_{e^-}(T1_{Se^-}) = \frac{N(T1_{Se^-} \otimes T2_\gamma)}{N(T2_\gamma)} \frac{(1 + \alpha_{Tot}(T1))}{\alpha_S(T2)} \quad (6)$$

In these expressions, $N(T2_{Se-})$ and $N(T2_\gamma)$ are the total number of internally converted electrons from the

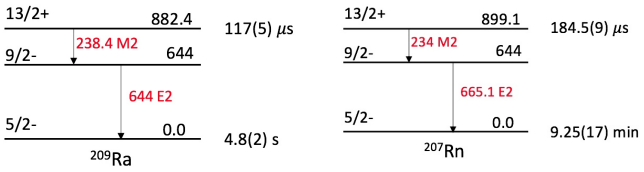

(a) (b)

Figure 7: Partial level schemes of a) ^{209}Ra [27] and b) ^{207}Rn [28] showing the low-lying $\frac{13}{2}^+$ isomers, whose decays have been used to validate the GEANT4 simulations.

S shell and gamma rays detected from the T2 transition in the corresponding singles spectra.

Following this procedure, the efficiency values extracted from the simulations are given in table 4 and found to disagree with the expected values of figs. 6a and 6b obtained by simulating individual gamma rays and electrons. This discrepancy can be attributed solely to summing in the detectors. Indeed, the 238.4 keV gamma ray can sum with the 644 keV gamma ray. Each of the gamma rays can also sum with X rays emitted in the atomic relaxation process following the internal conversion of the other transition or with X rays emitted by the BGO shields. In the Compton suppressed mode, full-energy events in one detector may be suppressed when other gamma rays enter the BGO shield and deposit energy above the detection threshold. Similarly, summing of conversion electrons with other conversion electrons, Auger electrons, or X rays can occur in the tunnel detectors.

In the singles method, the gamma-ray efficiencies can be corrected by excluding the influence of one transition on the other. In principle, this correction should be applied per detector as the detection probability of every detector is different

$$\varepsilon_\gamma(T1_\gamma) = \sum_{i}^{no.\,of\,detectors} \frac{N^i_{peak}(T1_\gamma)}{N_{emitted} \times (1 - \varepsilon^i_{Tot}(T2))} \quad (7)$$

where $\varepsilon^i_{Tot}(T2)$ is the detection probability in detector i of any radiation emitted in $T2$. This probability is obtained by simulating the decay of $T2$ alone.

Similar corrections can be applied to the electron efficiencies as well, however, due to a relatively large number of strips involved, this correction was not carried out in our study.

In the coincidence method, corrections can be made by integrating the peaks formed due to summing. As an example, consider the coincidence between K converted electrons (Ke^-) from the 238.4 keV transition and gamma rays from the 644 keV transition, they are denoted by $644_\gamma \otimes 238.4_{Ke^-}$ in the gamma-electron coincidence matrix shown in fig. 10. The Ke^- of the 238.4 keV transition are seen not only in coincidence with 644 keV gamma rays but also with gamma-ray events of apparent energies of 644 + KX rays. The modified gamma-ray efficiency equation for a given transition is then, to first order, given by:

$$\varepsilon_\gamma(T1_\gamma) = \frac{\Delta N}{N(T2_{Ke^-})}(1 + \alpha_{Tot}(T1)) \quad (8)$$

where,

$$\Delta N = N(T1_\gamma \otimes T2_{Ke^-}) + N((T1_\gamma + KXrays) \otimes T2_{Ke^-})$$

$$\Delta N(T1_K) = N(T2_\gamma)\frac{\alpha_K(T1)}{(1 + \alpha_{Tot}(T1))} \times \varepsilon^t_{Ke^-}(\omega_K \varepsilon^t_{KXrays} + a_K \varepsilon^t_{KAuger}) \quad (9)$$

where , $\varepsilon^t_{Ke^-}$ is the probability of detecting a Ke^- in the tunnel detector with full energy, ω_K and a_K are the fluorescence and Auger yields following a K shell vacancy in Ra, and, ε^t_{KXrays} and ε^t_{KAuger} are the full-energy peak efficiency of KX rays and KAuger electrons in the tunnel detectors, respectively. These probabilities are obtained by simulating a single gamma ray and an electron with weighted mean KX-ray energy (74.76 keV) and KAuger electron energy (90.63 keV) of Ra respectively. There is also summing of partial energy depositions of L converted electrons with the X rays following L vacancies, which yields counts in the full energy peak, which must also be subtracted. This increase is calculated by:

$$\Delta N(T1_L) = N(T2_\gamma)\frac{\alpha_L(T1)}{(1 + \alpha_{Tot}(T1))}\varepsilon^t_{Le^-}(C_{L1}+C_{L2}+C_{L3})$$

$$C_{L1} = \omega_{L1}\varepsilon^t_{L1Xrays} + f_{12}(\omega_{L2}\varepsilon^t_{L2Xrays} + f_{23}\omega_{L3}\varepsilon^t_{L3Xrays}) + f_{13}\omega_{L3}\varepsilon^t_{L3Xrays}$$
$$C_{L2} = \omega_{L2}\varepsilon^t_{L2Xrays} + f_{23}\omega_{L3}\varepsilon^t_{L3Xrays}$$
$$C_{L3} = \omega_{L3}\varepsilon^t_{L3Xrays}$$

where similarly, $\varepsilon^t_{Le^-}$ is the probability of detecting an Le^- in the tunnel detector with full energy, ε^t_{iXray} is the absolute detection efficiency of the tunnel detectors for X rays emitted from the Li subshell determined from simulations, ω_{Li} is the fluorescence yield of subshell Li (see table 2), and f_{12},f_{13}, f_{23} are Coster-Kronig yields taken from the TOI. Simulations showed that the efficiency to detect L1, L2 and L3 Auger electrons in the tunnel detectors is close to zero, hence their summing with Le^- is ignored. The efficiency equation then becomes:

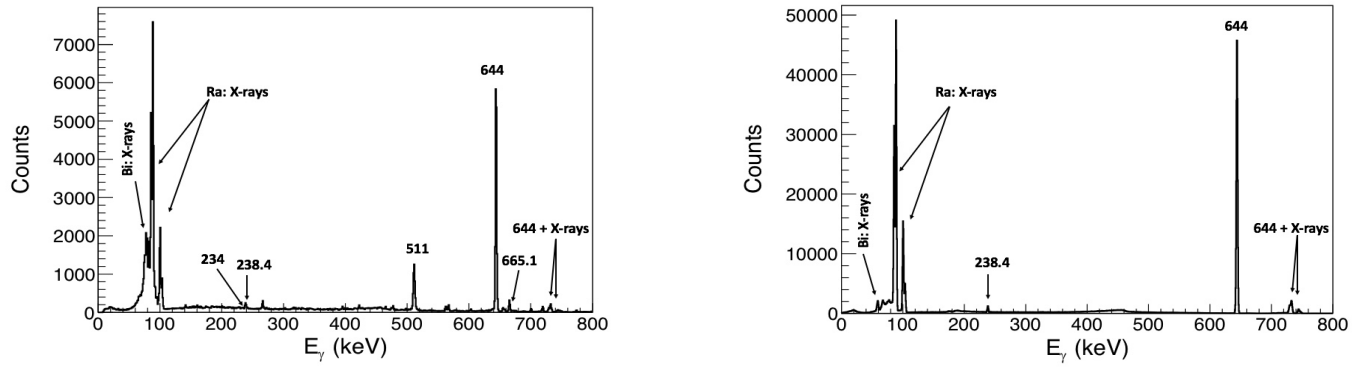

(a) (b)

Figure 8: a) Experimental and b) simulated spectrum of gamma rays emitted in the isomeric decay of ^{209}Ra.

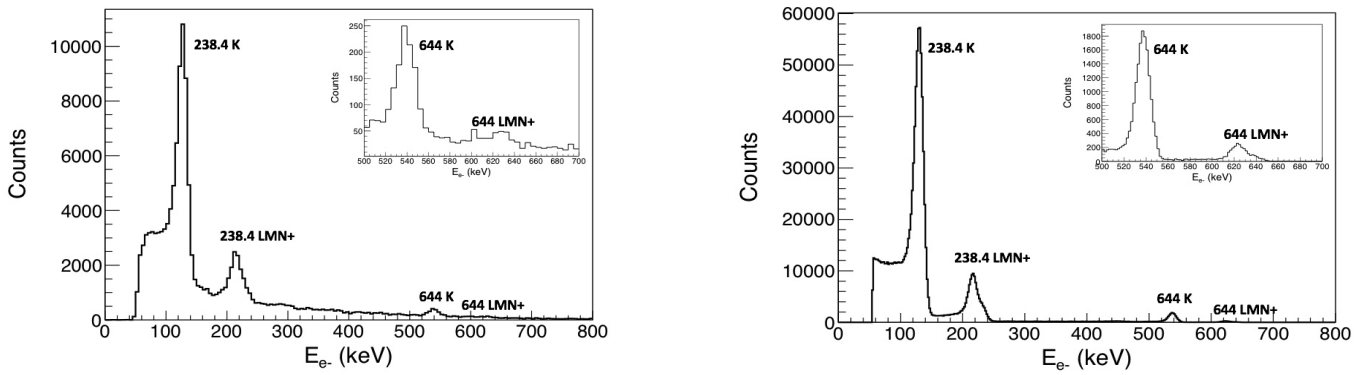

(a) (b)

Figure 9: a) Experimental and b) simulated spectrum of internal conversion electrons emitted in the isomeric decay of ^{209}Ra. The insets show zooms on the K and the LMN+ peaks of the 644 keV transition.

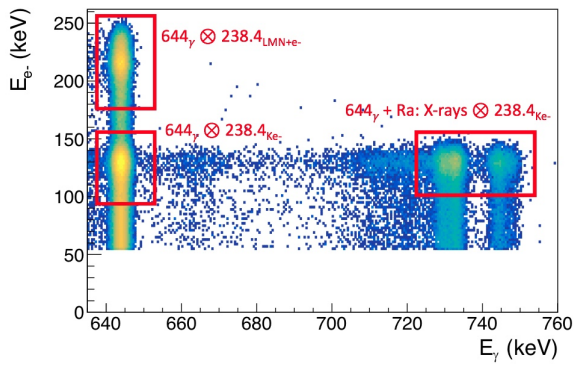

Figure 10: Selected region of the simulated gamma-ray and conversion electron coincidence matrix measured in the isomeric decay of ^{209}Ra.

subshell	energy (keV)	ε^t in (%)	ω
L1	15.74	22.63 ± 0.15	0.146
L2	15.82	22.63 ± 0.15	0.456
L3	9.59	24.54 ± 0.16	0.437

Table 2: The absolute detection efficiency of tunnel detector for X rays emitted from each subshell of L having intensity weighted energy. The fluorescence yield, ω is taken from TOI [23].

Accounting for all the summing contributions, the simulated efficiency values obtained by the singles and coincident methods are tabulated in table 4 and displayed in fig. 11. They are consistent with the efficiencies obtained by simulating individual electrons or

$$\varepsilon_{e^-}(T1_{LMN+e^-}) = \frac{N'}{N(T2_\gamma)} \frac{(1+\alpha_{Tot}(T1))}{\alpha_{LMN+}(T1)} \qquad (10)$$

where,

$$N' = N(T1_{LMN+e^-} \otimes T2_\gamma) - \Delta N(T1_K) - \Delta N(T1_L)$$

Shell	α (M2)	α (E2)
Tot	5.34±0.08	0.0216 ±0.0003
K	3.79 ± 0.05	0.0154 ± 0.0002

Table 3: Intensity-weighted conversion coefficients used in this work (see text for details).

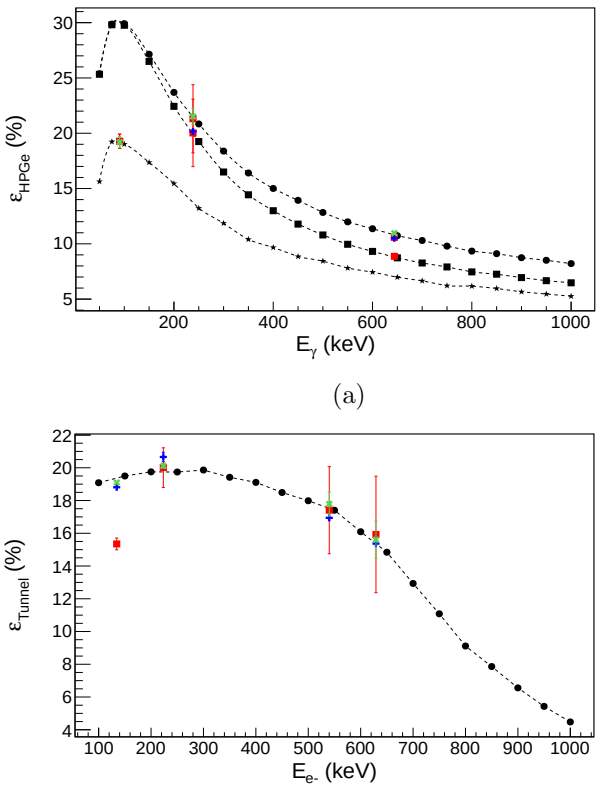

Figure 11: Absolute efficiency curves for the a) Ge and b) Tunnel detectors. a) ■ and ● denote the simulated efficiencies in singles and add back mode for the whole Ge array respectively. ★ represents the simulated efficiencies for the clover detector in the add back mode. b) ● represent the simulated e- efficiency for the 113 active strips during the ^{209}Ra calibration run. ✚ and ✖ correspond to the simulated efficiencies extracted from simulated ^{209}Ra isomeric data using the singles and coincidence methods. ■ correspond to the measured gamma-ray or electron efficiencies.

gamma rays (figs. 6a and 6b).

Summing in the detectors has one advantage, as it is possible to deduce the KX-ray efficiency of a Ge detector from the $\gamma_{detector\,i} - e^-$ coincidences using the following equation,

$$\varepsilon_\gamma(KXrays) = \frac{1}{\omega_K(\frac{N_\gamma}{N_{\gamma+Xrays}} + \frac{1}{P/T})} \qquad (11)$$

where N_γ is the number of counts in the T2 transition gamma-ray peak coincident with K shell electrons emitted in the T1 transition, $N_{\gamma+Xrays}$ is the number of counts in the peaks formed from summing of T2 gamma rays with KXrays radiated in the T1 transition and P/T denotes the peak-to-total ratio at the mean energy of the Ra X rays.

Note that in table 4, without correction for summing, the extracted value of the KX-ray efficiency is larger than the expected value. This is because the summing of Ke^- with the X rays and the Auger electrons in the tunnel detectors reduces the integral of the Ke^- peak. Hence the apparent number of gamma rays N_γ detected in coincidence with Ke^- is artificially reduced. The proper value is obtained by considering this.

A similar treatment was performed on the experimental data to extract the efficiency values with an added complications that the contribution from the isomeric decay of ^{207}Rn (the decay scheme is shown in fig. 7b) needed inclusion in the analysis. It is because the electrons emitted from the M2 transition in the isomer decay of ^{207}Rn and ^{209}Ra have quite similar energies and cannot be resolved in the tunnel detectors. Hence, intensity-weighted internal conversion coefficients (see table 3), fluorescence and Auger yields and KX-ray and Auger electron energies were used in the equations 8-11.

The experimentally measured efficiency values obtained using coincidence method are compatible with the simulation results (see the table 4 and fig. 11) except for the electron efficiency at $Ke^-(238.4)$ energy. This lower-than-expected value is due to a threshold effect, as some of the tunnel strips had higher thresholds than others. In our study, only the KX-ray efficiency of the clover detector was measured solely for statistical reasons. Also note that the large error bars in fig. 11 are due to low number of recorded 238.4 keV gamma-ray events in coincidence with 644_{Se^-}. We have also extracted from gamma-electron coincidences the addback factor of the clover detector at 644 keV in the simulated and the experimental data. The values were also found to be in good agreement 1.36 ± 0.01 (simulation) and 1.34 ± 0.05 (experimentally). This compatibility of the simulation and experimental results proves that the geometry of GABRIELA described in GEANT4 is quite accurate.

7 Conclusion

The current configuration of the GABRIELA detection system has been introduced. Using GEANT4 simulations the gamma-ray and electron detection efficiencies of this configuration have been presented. An overall increase in performance is observed compared to its previous version. We have validated the simulated efficiency curves using data from a calibration run, demonstrating that the geometry constructed in the GEANT4 code is accurate and can hence be reliably incorporated in the analysis and interpretation of experimental data. It was also demonstrated how simulations may be used to estimate the implantation depth of the evaporation residues in the implantation detector, which is crucial for determining

	Single gamma-ray or electron emission	Simulated ^{209}Ra isomeric decay				Experimental	
	Singles Method	Singles Method		Coincidence Method		Coincidence Method	
Energy (keV)	ε (%)	ε_0 (%)	ε^* (%)	ε_0 (%)	ε^* (%)	ε_0 (%)	ε^* (%)
Gamma							
KXrays (clover)	19.40±0.14	-	-	20.46±0.35	19.19±0.51	20.54±0.66	19.27±0.65
238.4	21.60±0.15	16.03±0.03	20.16±0.04	17.78±0.68	21.52±0.75	16.44±2.06	21.31±3.08
644	10.98±0.10	8.96±0.01	10.50±0.01	9.39±0.03	10.97±0.03	9.28±0.15	10.58±0.17
Electron							
134.48	19.04±0.14	18.81±0.02	-	17.72±0.07	19.10±0.07	15.48±0.24	15.35±0.36
223.48	20.15±0.14	20.66±0.29	-	25.46±0.11	20.13±0.12	24.09±0.39	20.03±1.21
540.08	17.71±0.13	16.94±0.11	-	18.06±0.73	17.79±0.73	18.70±2.59	17.41±2.66
629.25	15.30±0.12	15.37±0.16	-	19.73±1.12	15.61±1.13	19.79±4.18	15.93±3.56

Table 4: The measured gamma-ray and electron efficiency values obtained from singles and coincidence methods: ε corresponds to efficiency from a ^{209}Ra distributed source emitting either a single gamma or an electron isotropically with the given energy. ε_0 and ε^* indicate values extracted without or with summing corrections (see the text for details) for ^{209}Ra isomeric decay.

correctly the electron detection efficiency.

It has been shown that due to summing effects, the extraction of the absolute detection efficiency is quite challenging even for cascades of only two transitions. With an increasing number of coincident transitions, as can be the case, for example, in the decay of a high K isomer or of high-energy excited states populated by alpha decay, performing a similar correction procedure may not be straightforward and can be quite cumbersome, especially since the transitions involved may not be pure or of unknown electromagnetic character. It would be erroneous to establish decay schemes based solely on the gamma-ray and conversion electron efficiency-corrected intensities. Since the internal conversion process becomes the dominating decay mode in the heavy region, more summing is expected due to atomic relaxation processes, as a result, making the study of heavy nuclei difficult. Thus, in a compact and efficient spectrometer such as GABRIELA, it is imperative to perform simulations and compare with the experimental results in order to establish decay properties of heavy nuclei.

Acknowledgement

This work was supported by the Russian Foundation for Basic Research (projects nos. 18-52-15004), the French national Research Agency (projects nos. ANR-06-BLAN- 0034-01 and ANR-12-BS05-0013) and the IN2P3-JINR collaboration agreement no. 04-63.

References

[1] K. J. Moody, *The Chemistry of Superheavy Elements*, 1, 2nd ed.(Springer, Berlin, Heidelberg, 2014).

[2] R.-D. Herzberg, *The Chemistry of Superheavy Elements*, 83, 2nd ed. (Springer, Berlin, Heidelberg, 2014).

[3] Yu. Ts. Oganessian and V. K. Utyonkov, Nucl. Phys. A **944**, 62 (2015).

[4] Ch. Theisen *et al.*, Nucl. Phys. A **944**, 333 (2015).

[5] K. -H. Schmidtet *et al.*, Phys. Lett. B **168**, 39 (1986).

[6] E. Paul *et al.*, Phys. Rev. C **51**, 78 (1995).

[7] M. Asai *et al.*, Nucl. Phys. A **944**, 308 (2015).

[8] K. Hauschild *et al.*, Nucl. Instr. Meth. A **560**, 388 (2006).

[9] A.G. Popeko *et al.*, Nucl. Instr. Meth. B **376**, 140 (2016).

[10] A. Lopez-Martens *et al.*, Phys. Rev. C **74**, 044303 (2006).

[11] K. Rezynkina *et al.*, Phys. Rev. C **97**, 054332 (2018).

[12] A. Lopez-Martens *et al.*, Eur. Phys. J. A **32**, 245 (2007).

[13] A. Lopez-Martens *et al.*, Nucl. Phys. A **852**, 15 (2011).

[14] K. Hauschild *et al.*, Phys. Rev. C **78**, 021302 (2008).

[15] K. Rezynkina, PhD Thesis, Université Paris Saclay, (2016).

[16] G. Duchêne *et al.*, Nucl. Instr. Meth. A **432**, 90 (1999).

[17] A. V. Isaev *et al.*, Instr. Exp. Tech. **54**, 1, 37 (2011).

[18] S. Agostinelli *et al.*, Nucl. Instr. Meth. A **506**, 250 (2003).

[19] Steffen Hauf *et al.*, IEEE Trans. Nucl. Sci. **60**, 4, 2966 (2013).

[20] http://www.nndc/bnl.gov/ensdf

[21] L. G. Sarmiento *et al.*, Nucl. Instr. Meth. A **667**, 26 (2012).

[22] L. G. Sarmiento, EPJ Web Conf. **131**, 05004 (2016).

[23] R.B. Firestone, V.S. Shirley, C.M. Baglin, F.Y.F. Chu and J. Zipkin, *Table of Isotopes* (John Wiley and Sons, New York 1996).

[24] J. F. Ziegler *et al.*, Nucl. Instr. Meth. B **268**, 1818 (2010).

[25] F.P. Heßberger *et al.*, Eur. Phys. J. A **30**, 561 (2006).

[26] R. Chakma *et al.*, *Decay Spectroscopy of* ^{255}*Rf and* ^{251}*No*, to be published.

[27] K. Hauschild *et al.*, Phys. Rev. C **77**, 047305 (2008).

[28] I. Rezanka *et al.*, Phys. Rev. C **10**, 766 (1974).

[29] J F C Cocks and JUROSPHERE Collaboration, J. Phys. G: Nucl. Part. Phys. **25**, 839 (1999).